1994ApJ...432..641G

THE ASTROPHYSICAL JOURNAL, 432:641–647, 1994 September 10
© 1994. The American Astronomical Society. All rights reserved. Printed in U.S.A.

THE FAR-ULTRAVIOLET DUST ALBEDO IN THE UPPER SCORPIUS SUBGROUP OF THE SCORPIUS OB2 ASSOCIATION

KARL D. GORDON AND ADOLF N. WITT
Ritter Astrophysical Research Center, The University of Toledo, Toledo, OH 43606

AND

GEORGE R. CARRUTHERS, SUSAN A. CHRISTENSEN, AND BRIAN C. DOHNE
E. O. Hulburt Center for Space Research, Code 7609, Naval Research Laboratory, Washington, DC 20375-5320
Received 1994 January 7; accepted 1994 March 15

ABSTRACT

During NRL's Far Ultraviolet Cameras experiment on STS-39, four images of the giant reflection nebula encompassing the Upper Scorpius subgroup of the Sco OB2 association were obtained in two ultraviolet bandpasses with $\lambda_{\rm eff} = 1362$ Å and 1769 Å. From these images and *IUE* and *TD-1* stellar spectra, the ratio of nebular to stellar flux was calculated. The ratio ranged from 0.577 to 0.921 at 1362 Å and 0.681 to 0.916 at 1769 Å with the spread in the ratio arising mainly from uncertainties in the sky background. In order to analyze these images, a model utilizing Monte Carlo techniques to describe radiative transfer in a spherical nebula with asymmetrically distributed stars was developed by elaborating on previous work by Witt (1977). This model was used to determine the range of albedos reproducing the observed nebular-to-stellar flux ratios while allowing the scattering phase function asymmetry to vary between 0.0 and 0.8. The resulting albedos were 0.47–0.70 at 1362 Å and 0.55–0.72 at 1769 Å.

Subject headings: dust, extinction — ISM: individual (Scorpius OB2) — open clusters and associations: individual (Scorpius OB2) — radiative transfer — ultraviolet: ISM

1. INTRODUCTION

The dust albedo in the far-ultraviolet (FUV), 912–2500 Å, has been studied by many authors, but agreement on the range of acceptable albedos has yet to be reached. The FUV albedo has been determined by measuring the spatial distribution of the diffuse galactic light (DGL) and the scattered light in reflection nebulae and interpreting these observations with radiative transfer models. Early work using the DGL concluded that the FUV albedo was approximately 0.6 (Witt & Lillie 1973; Lillie & Witt 1976). The latest work on the DGL has constrained the FUV albedo to be less than 0.25 (Hurwitz, Bowyer, & Martin 1991). An extensive multiwavelength study of the reflection nebula NGC 7023 concluded that the FUV albedo was greater than 0.6 (Witt et al. 1982; Witt et al. 1992; Witt et al. 1993). Bowyer (1991) and Henry (1991) have disagreed on the solution to the FUV albedo problem in two recent reviews concentrating on determinations using the DGL. Mathis (1993) gives an excellent general review of interstellar dust including a review of the two above reviews.

The disagreement surrounding the FUV albedo arises in the DGL from the coupled nature of the two parameters used to describe the scattering process which produces the scattered light intensity. The two parameters describing the scattering process are the albedo, the percentage of light reflected by the dust grain, and the scattering phase function asymmetry, g. The scattering phase function asymmetry is the weighted average of the cosine of the scattering angle, where the weight is the scattering phase function. This coupling arises in the interpretation of the high-latitude DGL intensity which can be produced by a low albedo and low g or a high albedo and high g. In studying reflection nebulae, this coupling is much weaker, but uncertainties in the nebula's geometry greatly affect the validity of the resulting FUV albedo.

Two classes of reflection nebulae exist, externally and internally illuminated. The distribution of surface brightness of an externally illuminated nebula is strongly dependent on g and only weakly dependent on the albedo (Witt & Stephens 1974; Witt, Oliveri, & Schild 1990). The total nebular flux of internally illuminated nebulae is strongly dependent on the albedo and only weakly dependent on g. As a result, observing externally illuminated nebulae probes g and internally illuminated nebulae probes the albedo.

The reflection nebula in the region of the Upper Scorpius subgroup of the Sco OB2 association is an internally illuminated nebula, thus allowing for a determination of the FUV albedo mostly independent of g. Studying this nebula avoids the main uncertainty associated with determinations of the FUV albedo from NGC 7023, namely foreground dust. Gaustad and Van Buren (1993) examined the *IRAS* database at the positions of O and B stars for extended objects with excess emission at 60 μm which indicated the presence of interstellar dust at that position. They deduce that we reside in a low-density "trough" in the interstellar medium which, in the direction of the Upper Scorpius subgroup of Sco OB2 association, extends out to 60 pc. Examining their data corresponding to the Upper Scorpius region, we find a hole in their "trough" in exactly the direction of the Upper Scorpius subgroup. There appears to be very little dust between us and the Upper Scorpius reflection nebula. The internal illumination arises from multiple embedded stars; thus the uncertainties associated with the physical properties of individual stars are averaged out. This nebula is in a quite different portion of the sky than previously studied nebulae, so our results will increase the applicability of comparing the average dust properties of nebulae with the dust properties of the DGL.

In § 2 we describe the observations of this nebula and the

© American Astronomical Society • Provided by the NASA Astrophysics Data System

1994ApJ...432..641G

calculation of the nebular to stellar flux ratio for this object. The model used in this study is explained in § 3. The application of the model to this specific nebula is detailed in § 4. In § 5 we discuss the ramifications of our results, and a summary of this paper appears in § 6.

2. OBSERVATIONS

Images of the Upper Scorpius subgroup of the Sco OB2 association were obtained during the Far UV Cameras experiment (NRL-803), which was part of the Air Force Space Test Program's AFP-675 payload that flew aboard the space shuttle in 1991 May (STS-39). The instrument consisted of two electrographic Schmidt cameras with opaque alkali halide photocathodes. The cameras had collecting aperture diameters of 75 mm with f/1 focal ratios. The first camera covered the wavelength range 1230–1600 Å using a CaF_2 filter. The second camera covered the range 1650–2000 Å using a SiO_2 filter and was equipped with a microchannel intensifier stage, which yielded an intensity gain of approximately 100. Each image extended over a circular area of 20° diameter with an angular resolution of approximately 3′ (Carruthers 1986). The images were digitized with a PDS model 1010 ms microdensitometer and calibrated using pre- and postflight measurements (Carruthers et al. 1992). The conversion from image pixels to Galactic coordinates was accomplished separately for each image by using the pixel coordinate of the intensity maxima of three unsaturated stars with known Galactic coordinates.

Four images were obtained with exposures between 30 and 300 s (Table 1). Image 4 taken with camera 2 for 30 s is displayed in Figure 1 (Plate 9). These images were centered on the star ρ Oph and contained a majority of the Upper Scorpius subgroup of the Sco OB2 association. In all four images, the light from the ultraviolet stars is scattered by the surrounding interstellar dust, producing a giant reflection nebula. These images are the first detailed FUV observations of this nebula and show a great deal of detail, including numerous dust lanes (Carruthers et al. 1992).

In order to compare these images with theoretical computations, the nebular to stellar flux ratio, F_N/F_S, was determined. The technique used to extract the nebular surface brightness, S_N, from the images was as follows: (1) each image was sliced along 16 parallel lines of constant Galactic latitude equally spaced in Galactic latitude, (2) the slices from images taken with the same camera were graphed together on a semilog plot increasing the visibility of the difference in the slopes of the stellar light and S_N, (3) a S_N curve was drawn removing the stellar light in the process, and (4) the S_N was determined at 16 points equally spaced in Galactic longitude. Two of these plots are displayed in Figures 2*a* and 2*b*. By plotting the slices from images taken with the same camera together, saturation problems were dealt with easily. Saturation was seen in some regions of images 1 and 3 and compensated for by using the corresponding unsaturated regions of images 2 and 4, respectively. For camera 1 an average shift of 2.4×10^6 photons (cm^2 s bandpass sr)$^{-1}$ between images 1 and 2 was found. This shift is most likely due to changes in the airglow, specifically O I $\lambda\lambda$1304–1356, as the shuttle moved around Earth in orbit. The saturation problems in addition to the lack of an accurate point-spread function for either camera, necessitated the visual extraction of S_N. This method of extraction introduced little error in the measurement of S_N as the angular size of these images relegated the majority of the image to pure nebular surface brightness. A generous estimate of the error in determining S_N from the semilog plots was 5×10^5 photons (cm^2 s bandpass sr)$^{-1}$.

The outcome of the extraction process was a 16×16 array of the nebular surface brightness for each camera. Each 16×16 array was expanded to fill a 512×512 array by linear interpolation between pixels and extrapolation on the very edges. This expansion was carried out simply to make the calculation of the nebular flux easier, i.e., each pixel was then small enough that its position alone determined if it was part of

TABLE 1

OBSERVATIONAL DETAILS

Image	Camera	Exposure Time (s)
1.....	1	300
2.....	1	100
3.....	2	100
4.....	2	30

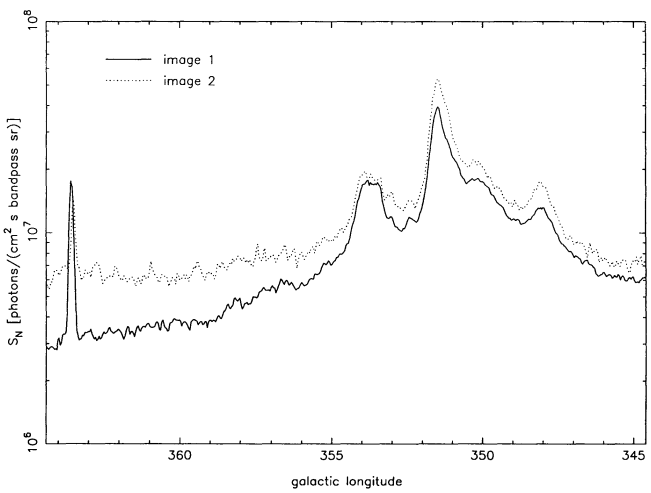

FIG. 2*a*

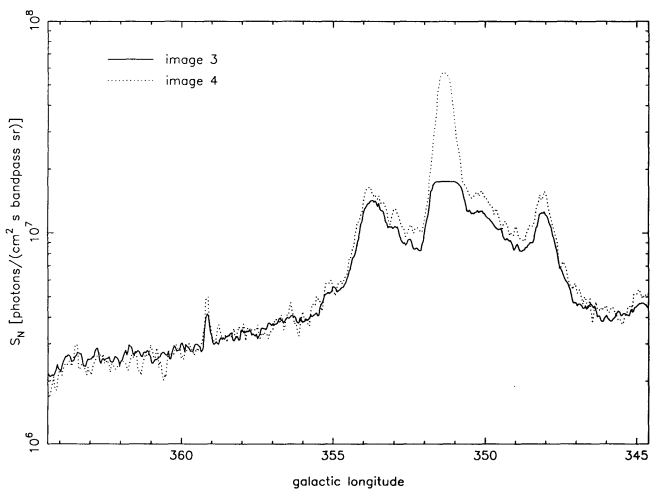

FIG. 2*b*

FIG. 2.—Nebular surface brightness slices (S_N) at $b = 17°.22$. (*a*) Images 1 and 2 both taken with camera 1. Note the calibration problem for this camera apparent in the shift of 2.4×10^6 photons (cm^2 s bandpass sr)$^{-1}$. (*b*) Images 3 and 4 both taken with camera 2. Note the saturation of image 3 between $l = 346°$ and 355°.

© American Astronomical Society • Provided by the NASA Astrophysics Data System

1994ApJ...432..641G

PLATE 9

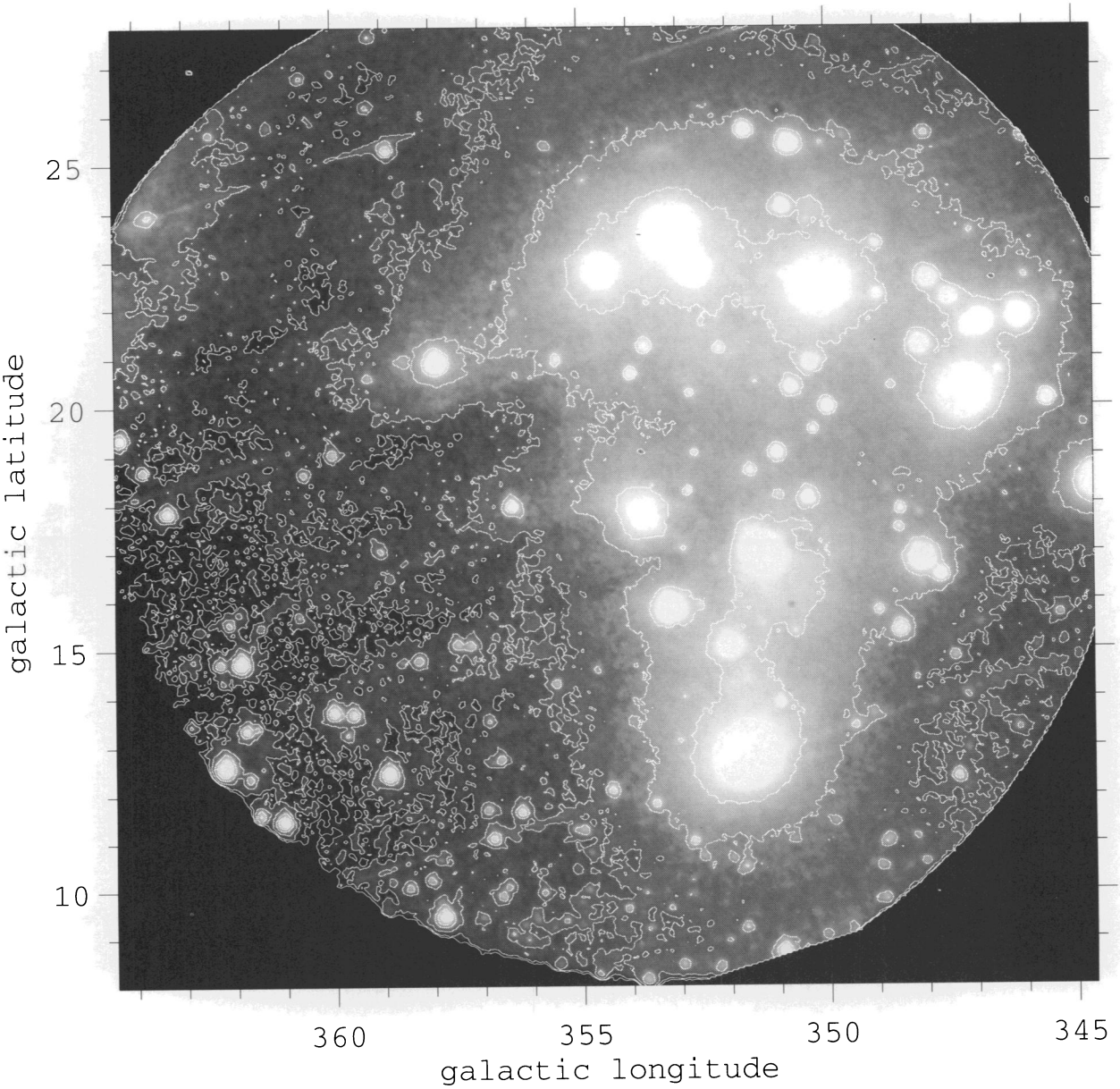

FIG. 1.—Image of the giant reflection nebula encompassing the Upper Scorpius subgroup of the Sco OB2 association in an ultraviolet bandpass with camera 2 and an exposure of 30 s. The isophotes are of log (S_N/F_S) and they begin with -0.5 sr^{-1}, increase in steps of 0.3 sr^{-1}, and end with 1.9 sr^{-1}. The image has been corrected for the maximum possible sky background, 1.8×10^6 photons (cm^2 s bandpass sr)$^{-1}$. The parallel linear streaks are trailed bright star images or scratches made as the film advanced.

GORDON et al. (see 432, 642)

© American Astronomical Society • Provided by the NASA Astrophysics Data System

1994ApJ...432..641G

the nebula. The calculation of the nebular flux, F_N, was then simply a matter of converting each pixel's surface brightness to a flux, subtracting the sky background, and adding up the fluxes within 9°.9 of the center of the image, $l = 354°.5$ and $b = 17°.9$. Since the nebula almost entirely filled the images, the sky background could not be determined precisely. Instead, constraints on the sky background were determined using the minimum nebular surface brightness as the maximum possible sky background and zero as the minimum sky background. For each camera, the range in F_N was calculated by using the 512 × 512 nebular surface brightness array and the constraints on the sky background (Table 3, cols. [5]–[6]). The error in the determination of the S_N translates into an error in F_N of $\Delta F_N = \Delta S_N \times \Omega = 4.68 \times 10^4$ photons (cm^2 s bandpass)$^{-1}$ where Ω is the solid angle of the nebula.

The composite stellar flux for each bandpass was determined by identifying the bright ultraviolet stars, convolving their spectral energy distributions with each camera's sensitivity function (Carruthers 1986), and summing the resulting fluxes. Using the ANS catalog of point sources (Wesselius et al. 1982), the bright stars were defined as stars with magnitudes brighter than 6 in the ANS bandpasses' 15W or 18. Basic data on these stars was collected from the literature (Table 2). The stars' spectra were taken from the *IUE* archives or the *TD-1* catalog (Thompson et al. 1978), giving preferences to large-aperture low-dispersion *IUE* spectra, then large-aperture high-dispersion *IUE* spectra, and finally *TD-1* data. While there is some question as to the accuracy of the faint *TD-1* fluxes (Gondhalekar 1990; Bowyer et al. 1993), the only star in this study needing *TD-1* fluxes was bright enough to avoid this difficulty. The composite stellar flux for each bandpass was computed by simply summing the individual stars' fluxes (Table 3, col. [4]). The effective wavelength, $\lambda_{\rm eff}$, and bandpass, $\Delta\lambda_{\rm eff}$, for each camera was calculated by weighting each star's $\lambda_{\rm eff}$ and $\Delta\lambda_{\rm eff}$ by the effective flux at $\lambda_{\rm eff}$ and the effective bandpass flux, respectively (Table 3, cols. [2]–[3]). The composite stellar flux of each bandpass was combined with the range of nebular fluxes yielding a range of F_N/F_S for each bandpass (Table 3, cols [7]–[8]). The error in the F_N/F_S was 0.041 for camera 1 and 0.065 for camera 2.

3. MODEL

Our model uses Monte Carlo techniques in determining the transfer of radiation through a spherical dust geometry. The dust geometry is broken into spherical shells allowing any radial distribution of dust, such as a geometry with a spherical dust shell and an inner dust-free region. The amount of dust is specified by the radial optical depth. The sources of emission are specified by their positions and luminosities, i.e., allowing multiple stars with an asymmetric distribution. In determining when and how a photon and a dust grain interact, the methods described in Witt (1977) are used.

TABLE 2

BASIC STELLAR DATA

HD	Name	l^{II} [°]	b^{II} [°]	MK[a]	Flux[b] [1362 Å]	Flux[b] [1769 Å]	Flux origin
141637	1 Sco	346.099	21.706	B1.5Vn	15150	10770	swp42216 & lwp20988
142096	λ Lib	350.72	25.38	B3V	7929	5644	swp42326 & lwr10778
142114	2 Sco	346.879	21.614	B2.5Vn	14710	9847	*TD-1*
142165	···	347.519	22.148	B5V	3066	2598	swp42217 & lwp17717
142184	···	347.934	22.545	B2V	5028	3731	swp36741 & lwp15993
142250	···	345.570	20.005	B7V	1845	1546	swp36742 & lwp15994
142301	3 Sco	347.1	21.51	B8III/IV	2227	2094	swp21092 & lwr16825
142315	···	348.982	23.299	B9V	422	393	swp36837 & lwp16118
142378	47 Lib	351.648	25.658	B2/3V	3178	2457	swp9236 & lwr7996
142883	···	350.886	24.086	B3V	2404	1904	swp42218 & lwp20990
142884	···	348.965	22.254	B8/9III	595	601	swp36743 & lwp15995
142990	···	348.121	21.197	B5V	4843	4099	swp42227 & lwp20991
143018A-B	π Sco	347.217	20.231	B1V+B2V	183800	115200	swp35530 & lwp15011
143275	δ Sco	350.099	22.491	B0.2IV	226100	148300	swp35532 & lwp15012
144217-8	β1-2 Sco	353.195	23.600	B0.5V+B2V	169400	99370	swp36791
144334	···	350.349	20.855	B8V	2350	2157	swp21083 & lwr16819
144470	ω1 Sco	352.752	22.773	B1V	34040	23220	swp42228 & lwp20992
144661	···	349.996	19.969	B8IV/V	1418	1222	swp13953
144844	···	350.736	20.368	B9V	1240	1156	swp36828 & lwp16109
145482	13 Sco	348.118	16.836	B2V	25220	17130	swp19351
145483	12 Sco	347.747	16.498	B9V	1113	1209	swp16306
145501	ν Sco C	354.616	22.711	B8/9V	723	661	swp7901 & lwr6884
145502	ν Sco A	354.611	22.701	B2IV	26937	16074	swp29140
145792	···	351.012	19.029	B6IV	1444	1089	swp36749 & lwp16002
146001	···	350.389	18.118	B8V	1414	1146	swp38567 & lwp16003
146416	···	353.983	20.598	B9III/IV	450	466	swp36831 & lwp16112
147165	σ Sco	351.315	16.999	B1III	47550	26160	swp45517 & lwp23843
147933-4	ρ Oph A & B	353.688	17.687	B2/3V+B2V	9564	6396	swp6588 & lwr5639
148184	χ Oph	357.677	20.677	B2Vne	8827	5955	swp15059
148479	α Sco B	351.95	15.06	B2.5V	3449	2471	swp41472 & lwp20233
148605	22 Sco	353.100	15.796	B3V	13970	10100	swp9221 & lwr7977
149438	τ Sco	351.536	12.808	B0V	321300	193800	swp33008 & lwp12766

[a] Houk 1982; Houk & Smith-Moore 1988.

[b] Units: photons (cm^2 s bandpass)$^{-1}$.

© American Astronomical Society • Provided by the NASA Astrophysics Data System

1994ApJ...432..641G

TABLE 3

CALCULATED QUANTITIES FROM OBSERVATIONS

Camera (1)	λ_{eff} (Å) (2)	$\Delta\lambda_{eff}$ (Å) (3)	F_* (photons/[cm^2 s filter]) (4)	$(F_N)_{min}$[a] (photons/[cm^2 s filter]) (5)	$(F_N)_{max}$[b] (photons/[cm^2 s filter]) (6)	$(F_N/F_*)_{min}$ (7)	$(F_N/F_*)_{max}$ (8)
1.....	1362	270	1.142×10^6	6.587×10^5	1.052×10^6	0.577	0.921
2.....	1769	278	7.190×10^5	4.897×10^5	6.583×10^5	0.681	0.916

[a] Derived from the maximum possible sky background.
[b] Derived from a sky background of zero.

The total number of photons in a particular model calculation is divided up among the stars in the nebula according to each star's unreddened luminosity. Thus, each photon starts its journey from one of these stars. The photon experiences forced first scattering, with the appropriate reduction in its weight, and any subsequent scatterings are determined via Monte Carlo techniques. Throughout the photon's journey, the effects of all scatterings are noted by keeping a weight. Thus, when we speak of a photon and its weight we are speaking of a conceptual tool useful in determining the behavior of radiation as it travels through the dust cloud. The final weight of the scattered photon is

$$W_{\text{scattered}} = (1 - e^{-\tau})a^n\phi(\cos\theta, g)dw\ . \quad (1)$$

The term $(1 - e^{-\tau})$ accounts for the amount of the photon forced to scatter at the first scattering site where τ is the optical depth to the dust cloud's surface along the photon's initial direction. The term a^n accounts for the amount of the photon reflected from a dust grain for the total n scatterings, i.e., $(1 - a)^n$ is the amount of the photon absorbed by the dust. The term $\phi(\cos\theta, g)dw$ accounts for the amount of the photon actually impinging on a detector. It is composed of the normalized Henyey-Greenstein scattering phase function (Henyey & Greenstein 1941), where θ is the angle from the final scattering site such that the photon impinges on the detector, and dw the solid angle of the detector. Each photon's final weight, $W_{\text{scattered}}$, is binned according to its exit position on the surface of the dust cloud. This array of binned weights, which is an uncalibrated image of the nebular flux, is transformed into an image of the uncalibrated nebular surface brightness by dividing each array position by its solid angle. Summing all the elements of the uncalibrated nebula flux array results in the total nebula flux.

The weight of the part of each photon escaping the dust cloud without undergoing a single scattering is

$$W_{\text{stellar}} = e^{-\tau}\frac{dw}{4\pi}\ . \quad (2)$$

The term $e^{-\tau}$ accounts for the amount of the photon exiting the dust cloud without scattering at all where τ is the optical depth to the dust cloud's surface in the direction of the detector. The term $dw/4\pi$ accounts for the amount of the photon impinging on the detector. Each escaping photon's weight is summed to produce a composite stellar flux weight (F_S). The ratio F_N/F_S is a unitless number making it ideal for comparing observations with model calculations. Using the distribution of the nebular surface brightness and the composite stellar weight, the distribution of the ratio of the nebular surface brightness to stellar flux, S_N/F_S, is computed. This has units of sr^{-1}, making it an excellent way to compare the distribution of the nebular surface brightness with observations.

Our model has inputs of the albedo, phase function asymmetry, radial distribution of the dust, radial optical depth, and positions and luminosities of individual stars. The model produces the F_N/F_S and the distribution of the log (S_N/F_S). With slightly more work, a calibrated F_N and distribution of S_N can be also produced by knowing F_S in absolute units.

4. ANALYSIS

The result of this investigation was a derivation of the FUV albedo from the ratio F_N/F_S. We chose to study an optically thick nebula with embedded stars because the ratio F_N/F_S varies weakly with g. The actual distribution of scattered light does depend on g quite strongly, but the small variation of the total nebular flux with g is a direct result of the fact that the scattered light from the embedded stars emerges somewhere. The remaining inputs needed are the radial distribution of dust, the total optical depth, and the positions and luminosities of the embedded stars.

In the extensive survey of gas and dust in the Sco OB2 association by de Geus & Burton (1991) and de Geus (1992), the distribution of interstellar matter in the Upper Scorpius subgroup was, in a broad sense, found to be a roughly spherical shell with a projected radius of approximately 15° with a finger of denser matter piercing the shell. Our observations correspond to the lower portion of this shell, where this finger disrupts the shell. Thus, this conceptual picture is most uncertain in just the region of interest to us. Other studies have dealt with the ρ Oph molecular cloud in great detail, but as this cloud is only a small part of the Upper Scorpius subgroup, these studies were of marginal use for our purposes. In the absence of good spatial detail of the whole Upper Scorpius subgroup dust, the dust distribution was assumed to have a constant density, be spherically distributed, and centered on our observations. The radius was set to 9°.9 to correspond to the area in common to all of our observations. In an attempt to reconcile this simple dust distribution with the actual distribution, the stars were embedded in our spherical model nebula by their optical depths as detailed below.

In order to determine the radial optical depth of the nebula and the positions and luminosities of our stars, the effective optical depth toward each star was computed for both cameras' bandpasses. The effective optical depth was computed by

$$\tau_{\text{eff}} = \frac{\int \tau(\lambda)\text{Filter}(\lambda)\text{Flux}(\lambda)d\lambda}{\int \text{Filter}(\lambda)\text{Flux}(\lambda)d\lambda}\ , \quad (3)$$

where Filter(λ) is the camera sensitivity as a function of wavelength, and

$$\tau(\lambda) = \frac{E_{B-V}}{1.086}\left[\frac{E_{\lambda-2740}(\lambda)}{E_{B-V}} + \frac{A_{2740}}{E_{B-V}}\right]. \quad (4)$$

© American Astronomical Society • Provided by the NASA Astrophysics Data System

1994ApJ...432..641G

$E_{\lambda-2740}(\lambda)/E_{B-V}$ for each star was taken from Papaj, Wegner, & Krelowski (1991) for 15 of our stars and for the remaining stars an average constructed from these 15 stars was used (Table 4, col. [2]). Figure 3 plots this average along with the average for general interstellar matter. The E_{B-V} values were taken from de Geus, de Zeeuw, & Lub (1989) with the exception of HD 142096 and HD 142301, which were taken from Krelowski & Strobel (1983), and HD 148479 which was taken from Corbally (1984) (Table 4, col. [2]). The value of A_{2740}/E_{B-V} was determined from a characterization of extinction curves by their R_V values (Cardelli, Clayton, & Mathis 1988). In the absence of good R_V values for more than just a few of our stars, the value of R_V was chosen to be 3.5 using the logic that the majority of our stars possess the normal R_V, 3.2 and a minority possess much higher R_V's—notable those near the ρ Oph molecular cloud. The effective optical depths for each star are tabulated in Table 4, columns (3)–(4).

Using these optical depths, the radial optical depth and the stars' positions and luminosities were computed by the following procedure. The distance to the center of the nebula was assumed to be the average of the distances to the stars (de Geus et al. 1989), resulting in a distance of 149 pc. The stars were placed in the nebula along the line of sight defined by their Galactic coordinates to a depth corresponding to their optical depths. The nebular radial optical depth was taken to be the optical depth where all the stars just fit into our spherical model nebula. The nebular radial optical depths were 2.12 and 2.14 for camera 1 and camera 2, respectively. Thus, the stars are embedded correctly in optical depth space, but their physical depth position is not generally correct. Since nebular light depends more heavily upon the optical depth than the physical position of the stars, this should give an accurate result. The luminosities were then calculated from the distances to the stars' positions, as determined above, and dereddened fluxes calculated from the stars' observed spectral energy distribution (§ 2) and their extinction curves, detailed above. This ensured, the flux calculated from the model would be equivalent to the observed flux. In order to verify that our derived luminosities were not unreasonable, the luminosities at 1362 Å were converted to absolute ultraviolet magnitudes ($M_{1362\,\text{Å}}$) and compared to Carnochan's (1982) $M_{1400\,\text{Å}}$ indicated by the stars' MK classifications. As expected, the correspondence was not perfect; it produced a well-defined linear correlation with an average dispersion of 1.0 mag.

TABLE 4

STELLAR OPTICAL DEPTHS AND LUMINOSITIES

HD	E_{B-V}	τ_{eff} [1362 Å]	τ_{eff} [1769 Å]	L[c] [1362 Å]	L[c] [1769 Å]
141637[a]	0.153	0.885	1.068	65.2	42.2
142096[a]	0.23	1.684	1.591	76.6	38.6
142114[a]	0.113	0.985	0.802	63.0	26.9
142165[b]	0.113	0.806	0.782	10.7	6.8
142184[a]	0.153	1.172	1.116	26.6	14.5
142250[b]	0.050	0.357	0.346	4.0	2.6
142301[b]	0.07	0.499	0.485	5.4	3.9
142315[b]	0.117	0.832	0.810	1.5	1.0
142378[a]	0.138	0.972	0.907	13.4	7.5
142883[a]	0.172	1.344	1.196	14.9	7.8
142884[b]	0.159	1.128	1.100	2.9	2.2
142990[a]	0.091	0.816	0.760	16.4	10.1
143018A-B[a]	0.072	0.507	0.489	444.9	209.6
143275[a]	0.147	1.123	1.068	1069.7	509.1
144217-8[a]	0.172	1.228	1.154	889.9	375.3
144334[b]	0.081	0.578	0.561	5.7	4.0
144470[a]	0.219	1.469	1.510	237.0	132.2
144661[b]	0.097	0.692	0.672	3.9	2.6
144844[b]	0.116	0.826	0.803	4.0	2.8
145482[b]	0.044	0.316	0.304	46.4	24.1
145483[b]	0.059	0.418	0.409	2.3	2.0
145501[b]	0.247	1.757	1.709	6.9	5.2
145502[a]	0.247	1.682	1.581	234.7	109.4
145792[b]	0.169	1.207	1.168	7.2	4.0
146001[b]	0.153	1.091	1.058	6.2	3.8
146416[b]	0.075	0.532	0.520	1.0	0.8
147165[a]	0.375	2.579	2.410	1158.2	417.6
147933-4[a]	0.453	2.856	2.864	317.5	171.5
148184[a]	0.569	3.728	3.776	821.7	466.1
148479[b]	0.06	0.430	0.415	6.9	3.7
148605[b]	0.069	0.495	0.478	29.6	16.3
149438[b]	0.034	0.244	0.235	535.1	246.6

[a] Extinction curve from Papaj et al. 1991.
[b] Average extinction curve from above curves.
[c] Units: 1.559×10^{53} photons (s bandpass)$^{-1}$.

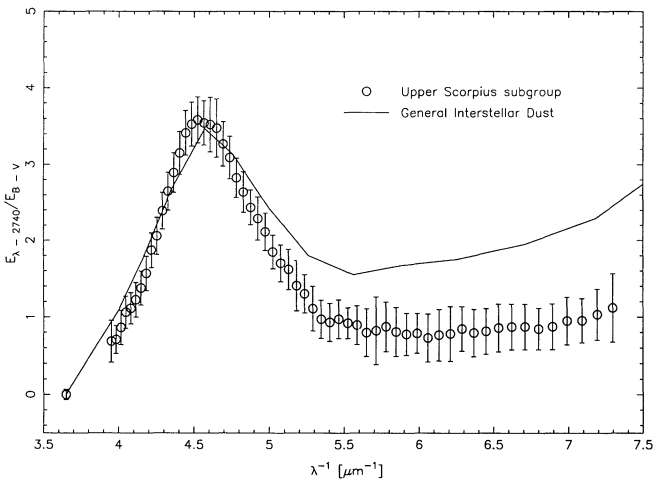

FIG. 3.—Extinction curves for the Upper Scorpius subgroup of the Sco OB2 association and the general interstellar dust (Whittet 1992). The extinction curve for the Upper Scorpius subgroup is an average of 15 stars in the subgroup (Papaj, Wegner, & Krelowski 1991).

With the necessary model inputs determined, we ran our model for an appropriate range of g's, 0.0–0.8, and calculated the albedo necessary to reproduce the observed range of the F_N/F_S for both cameras. The results are plotted in Figure 4. For camera 1 ($\lambda_{\text{eff}} = 1362$ Å), the FUV albedo ranged from 0.47 to 0.55 for the minimum F_N/F_S and from 0.64 to 0.70 for the maximum F_N/F_S resulting in a total range of 0.47–0.70. For camera 2 ($\lambda_{\text{eff}} = 1769$ Å), the FUV albedo ranged from 0.55 to 0.62 for the minimum $F_N F_S$ and from 0.66 to 0.72 for the maximum F_N/F_S resulting in a total range of 0.55–0.72. The error in the albedo from errors in determining the observed nebular surface brightness was 0.02 for camera 1 and 0.03 for camera 2. Notice that this error is much smaller than the uncertainty in the albedos introduced by the uncertainties in the sky background.

For completeness, we attempted to fit the observed distribution of S_N/F_S with the distribution of S_N/F_S calculated from our model. The calculated log (S_N/F_S) was compared to the observed log (S_N/F_S) by the linear least-squares method with a good fit defined as a slope of 1 and a y-intercept of 0. In Figure 5 we plotted the curves for a slope = 1, for a y-intercept = 0,

© American Astronomical Society • Provided by the NASA Astrophysics Data System

1994ApJ...432..641G

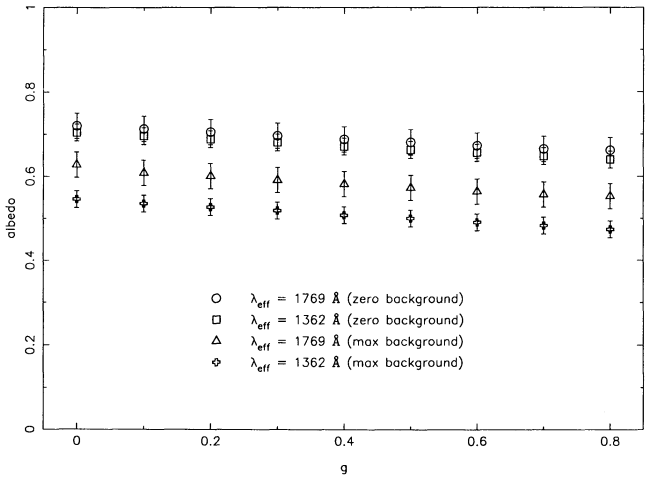

FIG. 4.—Plotted are albedos determined from our radiative model calculations. Note the small change in the albedo arising from allowing g to range between 0.0 and 0.8.

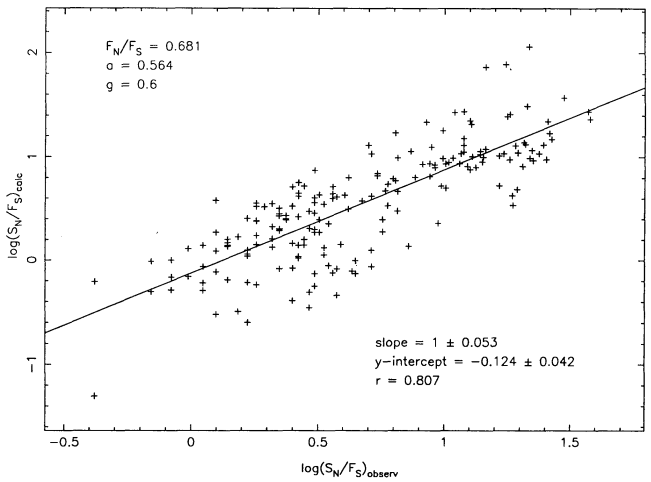

FIG. 6.—The plot of the observed vs. the calculated log (S_N/F_S) distribution and the linear least-squares fit. The y-intercept is not zero, but not far from zero.

and for a $F_N/F_S = 0.681$ (max background) for camera 2. This turned out to be the only case where the slope curve intersected. For the other three cases (camera 1, max background; camera 1, zero background, and camera 2, zero background,) none of the curves intersected. The intersect in Figure 5 between the slope and F_N/F_S curves occurs at a g of 0.6 and an albedo of 0.56. Figure 6 shows the observed versus calculated log (S_N/F_S) for this case. This result was quite surprising given our choice of such a simple geometry, i.e., a constant density sphere. The fact that none of the curves intersected for camera 1 might be related to the problems in the calibration of that camera but primarily reflects the fact that all these curves are only weakly dependent on g and are more or less parallel to each other within a narrow range of albedo values.

5. DISCUSSION

The main conclusion of this paper is that the FUV albedo is high. Specifically, at 1362 Å the range in albedos is 0.47–0.70 and at 1769 Å the range in albedos is 0.55–0.72. This result is independent of the choice of g but dependent on our choice of a spherical nebula with constant density and the absence of any foreground dust. The choice of such a simple nebular geometry was necessitated by the lack of sufficient observations. The fact that a good fit to the distribution of S_N/F_S is possible for even one case (camera 2, max background) allows us to conclude that while this may not be the actual geometry of the nebula, it is a good approximation. While we assumed a constant density for the nebula, this assumption was partially corrected by embedding the stars to a depth equal to their observed optical depths. The assumption of no foreground dust is realistic as we reside in a low-density "trough" in the interstellar medium (Gaustad & Van Buren 1993). The presence of any foreground dust would increase the albedo since more light would have to be reflected at each scattering to get the same F_N/F_S from a nebula with less dust, i.e., fewer scatterings implying a larger albedo. Thus, the FUV albedo must be high.

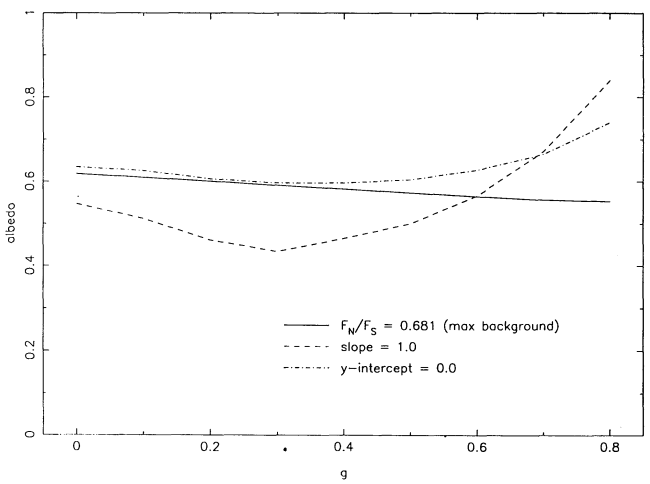

FIG. 5.—Curves for three different methods of determining the best fit to the observations for camera 2 with the maximum background. The solid line was determined by requiring the F_N/F_S of the model to match the observed F_N/F_S. The dashed line was determined from requiring the slope equal one of a least-squares fit between the observed and calculated values of log (S_N/F_S). The dot-dashed line was determined by requiring the y-intercept equal zero.

Assuming that the albedo of this nebula is not radically different than the albedo elsewhere in our Galaxy allows us to use the results of FUV DGL investigations. These investigations have concluded that either there is a high albedo and high g or a low albedo and low g. As we have shown that albedo is high, it immediately follows that g is also high. A high value of g, increasing with decreasing wavelengths in the FUV, was also indicated by the analysis of data for the reflection nebula NGC 7023 (Witt et al. 1992, 1993). This is born out by our attempt to fit the distribution of S_N/F_S with our model. The case where this was possible resulted in a high g (Figs. 5–6). Using the results of this fit, we ran our model to obtain an image of the nebula for comparison to the observations at $\lambda_{\rm eff} = 1769$ Å (Fig. 7 [Pl. 10]). Comparison between the observed image (Fig. 1) and the calculated image (Fig. 7) is not one-to-one as the observed image contains both stellar and nebular light while the calculated image contains only the nebular light. Overall, the distribution of nebular surface brightness corresponds fairly well. The bright stars are the same on both images and so is the general shape of the nebula.

In Figure 8, we compare our results with the results of other investigations which have also concluded that the FUV albedo is high. In addition, Figure 8 also contains both the normalized

© American Astronomical Society • Provided by the NASA Astrophysics Data System

1994ApJ...432..641G

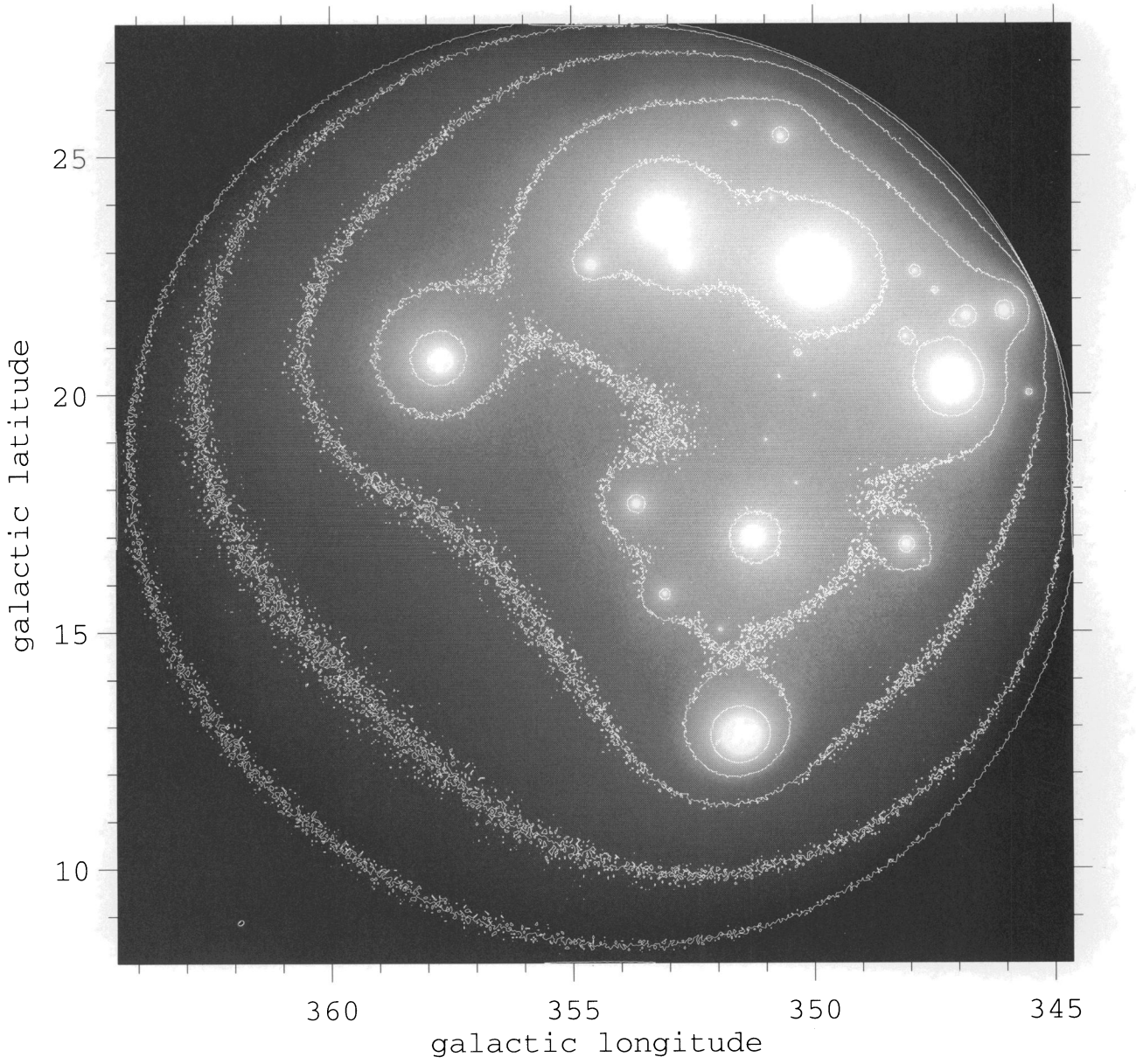

FIG. 7.—Image of the giant reflection nebula encompassing the Upper Scorpius subgroup of the Sco OB2 association calculated from our Monte Carlo model with albedo = 0.56 and $g = 0.60$. The isophotes are of $\log(S_N/F_S)$ and they begin with $-0.5\ \mathrm{sr}^{-1}$, increase in steps of $0.4\ \mathrm{sr}^{-1}$, and end with $1.9\ \mathrm{sr}^{-1}$. Note this image only includes nebular light while the image in Fig. 1 includes both nebular and stellar lights. A total of 2.13×10^9 photons were involved in calculating this image (512×512 pixels).

© American Astronomical Society • Provided by the NASA Astrophysics Data System

1994ApJ...432..641G

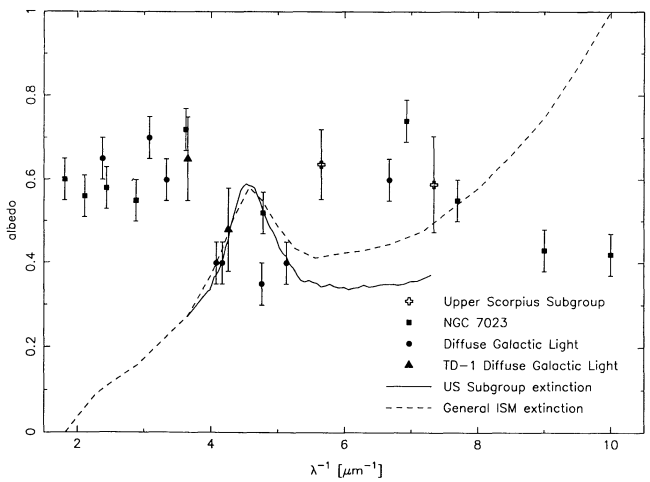

FIG. 8.—Our results plotted with the results of other investigations also finding the albedo to be high. The results for NGC 7023 are from Witt et al. (1982, 1992, 1993). The results for the diffuse galactic light are from Lillie & Witt (1976). The results for the *TD-1* diffuse galactic light are from Morgan, Nandy, & Thompson (1976). The general ISM extinction curve is from Whittet (1992).

general interstellar extinction curve (Whittet 1992) and the normalized average extinction curve for the Upper Scorpius subgroup of the Sco OB2 association. The decrease in the albedo in the wavelength range of the 2200 Å "bump" implies that the "bump" is definitely an absorption feature. In addition, note that our result for the slightly higher albedo at 1769 Å ($\lambda^{-1} = 5.6$ μm) implies there is no additional absorption from the "bump" which is expected based on the narrower 2200 Å "bump" seen in the extinction curve for our region. The correspondence between the albedo and the extinction curve is discussed in Witt et al. (1993).

6. SUMMARY

Four far-UV images of the giant reflection nebula encompassing the Upper Scorpius subgroup of the Sco OB2 association were obtained during the STS-39 Far Ultraviolet Cameras experiment in 1991 May. The images were obtained in two ultraviolet bandpasses with $\lambda_{\rm eff} = 1362$ Å and $\lambda_{\rm eff} = 1769$ Å. The distribution of the nebular surface brightness was extracted from two of the images in each wavelength range and the stellar flux from the bright ultraviolet stars was obtained from the *IUE* or *TD-1* archives. The nebular to stellar ratio was calculated for both bandpasses. Due to the fact that the reflection nebula extended over almost the entire image, it was possible to put constraints only on the sky background. This gave rise to a significant uncertainty in the observed nebular to stellar flux ratio derived from these images.

A radiative transfer model based on Monte Carlo techniques which allowed for an asymmetric distribution of stars inside a spherical nebula was created. The specific geometry of the Upper Scorpius reflection nebula was assumed to be a constant density sphere due to the lack of observations with sufficient detail. The stars were embedded in this geometry to a depth equal to their optical depths which were determined from known E_{B-V} and extinction curves from Papaj, Wegner, & Krelowski (1991).

As the ratio of nebular to stellar flux of an internally illuminated reflection nebulae is strongly dependent upon the albedo and only weakly dependent upon g, the model was run for a range of g's, 0.0–0.8, and the albedo fitting the observed nebular to stellar flux ratio was determined. The albedo was high and ranged from 0.47 to 0.70 for $\lambda_{\rm eff} = 1362$ Å and from 0.55 to 0.72 for $\lambda_{\rm eff} = 1769$ Å. The range in the albedos arose primarily from the uncertainty in the sky background. In an attempt to fit the observed distribution of S_N/F_S, we found that only one case resulted in a good fit, $\lambda_{\rm eff} = 1769$ Å with the maximum background. This fit was for a g of 0.60 and an albedo of 0.56.

We would like to thank J. Krelowski for providing us with the digital form of the extinction curves from Papaj et al. (1991). K. D. G. and A. N. W. acknowledge the support from NASA LTSAP grant NAGW-3168. We also thank the Air Force Space Test Program, NASA, The Office of Naval Research, and our co-workers at NRL for their support of the Far UV Cameras development and flight.

REFERENCES

Bowyer, S. 1991, ARA&A, 29, 59
Bowyer, S., Sasseen, T. P., Lampton, M., & Wu, X. 1993, ApJ, 415, 875
Cardelli, J. A., Clayton, G. C., & Mathis, J. S. 1988, ApJ, 329, L33
Carnochan, D. J. 1982, MNRAS, 201, 1139
Carruthers, G. R. 1986, Proc. SPIE—Ultraviolet Technology, 687, 11
Carruthers, G. R., Morrill, J. S., Dohne, B. C., & Christensen, S. A. 1992, Proc. SPIE—Ultraviolet Technology IV, 1764
Corbally, C. J. 1984, ApJS, 55, 657
de Geus, E. J. 1992, A&A, 262, 258
de Geus, E. J., & Burton, W. B. 1991, A&A, 246, 559
de Geus, E. J., de Zeeuw, P. T., & Lub, J. 1989, A&A, 216, 44
Gondhalekar, P. M. 1990, in IAU Symp. 139, Galactic and Extragalactic Background Radiation—Optical, Ultraviolet, and Infrared Components, ed. S. Bowyer & C. Leinert (Dordrecht: Kluwer), 449
Gaustad, J. E., & Van Buren, D. 1993, PASP, 105, 1127
Henry, R. C. 1991, ARA&A, 29, 89
Henyey, L., & Greenstein, J. 1941, ApJ, 93, 70
Houk, N. 1982, Michigan Catalogue of Two-Dimensional Spectral Types for the HD Stars, 3 (Ann Arbor: Braun-Brumfield)
Houk, N., & Smith-Moore, M. 1988, Michigan Catalogue of Two-Dimensional Spectral Types for the HD Stars, 4 (Ann Arbor: Braun-Brumfield)
Hurwitz, M., Bowyer, S., & Martin, C. 1991, ApJ, 372, 167
Lillie, C. F., & Witt, A. N. 1976, ApJ, 208, 64
Krelowski, J., & Strobel, A. 1983, A&A, 127, 271
Mathis, J. S. 1993, Rep. Prog. Phys., 56, 605
Morgan, D. H., Nandy, K., & Thompson, G. I. 1976, MNRAS, 177, 531
Papaj, J., Wegner, W., & Krelowski, J. 1991, MNRAS, 252, 403
Thompson, G. I., Nandy, K., Jamar, G., Monfils, A., Houziaux, L., Carnochan, D. J., & Wilson, R. 1978, Catalogue of Stellar Ultraviolet Fluxes (n.p.: The Science Research Council)
Wesselius, P. R., van Duinen, R. J., de Jonge, A. R. W., Aalders, J. G. W., Luinge, W., & Wildeman, K. J. 1982, A&AS, 49, 427
Whittet D. C. B. 1992, Dust in the Galactic Environment (Bristol: IOP)
Witt, A. N. 1977, ApJS, 35, 1
Witt, A. N., & Lillie, C. F. 1973, A&A, 25, 397
Witt, A. N., Oliveri, M. V., & Schild, R. E. 1990, AJ, 99, 888
Witt, A. N., Petersohn, J. K., Bohlin, R. C., O'Connell, R. W., Roberts, M. S., Smith, A. M., & Stecher, T. P. 1992, ApJ, 395, L5
Witt, A. N., Petersohn, J. K., Holberg, J. B., Murthy, J., Dring, A., & Henry, R. C. 1993, ApJ, 410, 714
Witt, A. N., & Stephens, T. C. 1974, AJ, 79, 948
Witt, A. N., Walker, G. A. H., Bohlin, R. C., & Stecher, T. P. 1982, ApJ, 261, 492

© American Astronomical Society • Provided by the NASA Astrophysics Data System